OPEN

Technical Basics and Clinical Benefits of Photon-Counting CT

Thomas Flohr, PhD, and Bernhard Schmidt, PhD

Abstract: Novel photon-counting detector CT (PCD-CT) has the potential to address the limitations of previous CT systems, such as insufficient spatial resolution, limited accuracy in detecting small low-contrast structures, or missing routine availability of spectral information. In this review article, we explain the basic principles and potential clinical benefits of PCD-CT, with a focus on recent literature that has grown rapidly since the commercial introduction of a clinically approved PCD-CT.

Key Words: computed tomography CT, photon-counting CT, photon-counting detector CT, spectral CT, CT coronary angiography, CT radiation dose, dual source CT

(*Invest Radiol* 2023;58: 441–450)

Computed tomography (CT) has undergone continuous technical development since its beginnings in the 1970s; today it is a mature radiological imaging method that has become the backbone of radiological diagnostics thanks to its speed and precise representation of anatomy. Over the course of its development, the scope of CT has gradually expanded from a purely morphological imaging technique to one that also includes various functional parameters, such as tissue perfusion.

Nevertheless, certain technical limitations of CT prevent an even wider expansion of its range of applications. Spatial resolution is still suboptimal for some demanding tasks, such as coronary CT angiography (cCTA) in patients with severe calcifications and stents. A recent study has shown that the performance of cCTA for the diagnosis of in-stent restenosis is still insufficient.[1] Accuracy in detecting small, low-contrast structures is limited; cancer may therefore be missed or wrongly diagnosed. As an example, a recent meta-analysis of studies showed that 22.5% of hepatocellular carcinomas are missed with CT.[2] Furthermore, findings in CT are sometimes ambivalent, such as high-density renal cysts; then, additional examinations must follow to obtain a clear diagnosis and to determine further clinical management. Further reduction of the radiation dose in CT remains a desirable goal. Despite all the technical progress, CT is still responsible for more than half of the dose of all diagnostic and interventional procedures.[3]

Novel photon-counting detector CT (PCD-CT), which has recently been introduced into clinical practice, has the potential to address these limitations and overcome the weaknesses of previous CT systems. Several review articles have been published explaining the basic principles and clinical advantages of PCD-CT with more or less technical depth, depending on the intended readership.[4–13] In this review, we will focus on recent literature that has grown rapidly since the commercial introduction of a clinically approved PCD-CT and on results from human examinations.

Received for publication December 31, 2022; and accepted for publication, after revision, March 5, 2023.

From the Department of Computed Tomography, Siemens Healthcare GmbH, Forchheim, Germany.

Conflicts of interest and sources of funding: Thomas Flohr and Bernhard Schmidt are employees of Siemens Healthcare GmbH.

Correspondence to: Thomas Flohr, PhD, Department of Computed Tomography, Computed Tomography, Siemens Healthcare GmbH, Siemensstr. 1, Forchheim D-91301, Germany. E-mail: thomas.flohr@siemens-healthineers.com.

ISSN: 0020-9996/23/5807–0441
DOI: 10.1097/RLI.0000000000000980

A BRIEF HISTORY OF PHOTON-COUNTING DETECTOR CT: FROM PRECLINICAL PROTOTYPES TO CLINICAL INTRODUCTION

Before describing the basics of PCD-CT, we will give a brief overview of the development of this new detector technology. We will skip benchtop setups or experimental devices and start with preclinical scanners that could be used to study humans.

The first preclinical prototype of a PCD-CT (GE Healthcare) was developed in 2008. Several studies on human volunteers demonstrated the clinical applicability of this new detection principle. The CT system used a 32-row cadmium-telluride, (CdTe) detector with 1×1 mm^2 detector pixels and 2 energy thresholds. It could only be operated with a lower radiation dose than clinically needed. Nevertheless, different types of dual-energy images could be computed.[14]

Starting in 2014, 3 preclinical prototypes of a hybrid dual-source PCD-CT, (SOMATOM CounT; Siemens Healthcare) were installed in clinical research environments. The prototypes were based on a clinical dual-source CT (SOMATOM Flash; Siemens Healthcare), with the smaller of the 2 detector arrays replaced by a CdTe PCD with a z-coverage of 16 mm at the isocenter.[15] It had subpixels with a size of 0.225×0.225 mm^2 and 2 energy thresholds. The subpixels were combined in various ways to form larger pixels or to allow the readout of 4 energy thresholds in a checkerboard arrangement with alternating low- and high-energy threshold settings. This prototype allowed for the first time scanning with typical clinical parameters, such as rotation times of 0.5 seconds and tube currents up to 550 mA. Extensive phantom and patient studies were carried out with these prototypes.[16] The noninferiority of PCD-CT compared with established clinical CT could be demonstrated and possible advantages as described later in this review were already pointed out.[17–19]

In 2017, a single-source PCD-CT prototype (Philips Healthcare) with a cadmium-zinc-telluride (CZT) detector was installed in a clinical research environment. It had a pixel size of 0.5×0.5 mm^2 and 5 energy thresholds. The shortest gantry rotation time was 1 second. This system was later upgraded to a preclinical PCD-CT with a field of view (FOV) of 50 cm, a z-coverage of 17.6 mm at the isocenter, and 0.33 seconds of gantry rotation time.[20] This system has been used for large animal and human studies, including cardiac CT.[21–24]

In 2020, the second generation of preclinical PCD-CT with a CdTe detector (SOMATOM CounT Plus; Siemens Healthcare) was installed at 3 clinical institutions. The single-source CT had 0.3 seconds gantry rotation time and was equipped with a detector consisting of subpixels with a size of 0.275×0.322 mm^2 (0.151×0.176 mm^2 at the isocenter). It provided a 50-cm FOV with a z-coverage of 57.6 mm at the isocenter and offered either 144×0.4 mm collimation with 2 energy thresholds or 120×0.2 mm collimation with 1 energy threshold.[7] The system was used to evaluate the performance and image quality of PCD-CT in a general clinical setting.[25]

Finally, in 2021, a first-generation PCD dual-source CT (PCD-DSCT) with 2 CdTe detectors was commercially introduced (NAEOTOM Alpha, Siemens Healthcare). Both detectors have a subpixel size of 0.275×0.322 mm^2 (0.151×0.176 mm^2 at the isocenter). The primary detector array covers a FOV of 50 cm diameter, and the second one has a FOV of 36 cm diameter. The shortest gantry rotation time is 0.25 seconds, corresponding to a temporal resolution of 66 milliseconds for ECG-controlled cardiac examinations; 2×2 subpixels can be combined into 1 macro-pixel; the system then offers data acquisition with 144×0.4 mm collimation and 4 energy thresholds for both detectors,

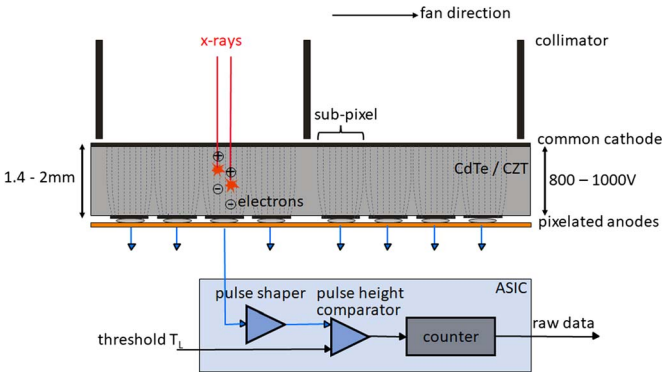

FIGURE 1. Schematic illustration of a CdTe/CZT PCD (top) and the corresponding read-out ASIC (bottom). View from the front of the CT system, the fan direction is the direction in the scan plane along the detector fan. The individual detector pixels are formed by the strong electric field between the common cathode and the pixelated anodes (indicated here by dashed lines); no further separation of the pixels, for example, by interlayers, is necessary. In the detector structure shown here, 4 subpixels each are located between 2 collimator blades to suppress scattered radiation, see also Figure 4. In the ASIC, the voltage pulses generated by the absorbed x-ray quanta are compared in a pulse height comparator with a threshold voltage corresponding to the desired threshold energy (20–25 keV). Only x-ray quanta exceeding this threshold energy are counted.

combined into 2 energy thresholds for routine applications. The subpixels can also be read out separately. Thereby, examinations with 120 × 0.2 mm collimation are possible, whereby one energy threshold is available with the maximum spatial resolution. Spectral images from 2 energy thresholds can additionally be reconstructed with the spatial resolution of the macropixels. The CT system is equipped with 2 x-ray tubes with 120 kW each and several focal spots, the smallest one with a size of 0.4 × 0.4 mm^2 (0.181 × 0.181 mm^2 at the isocenter). Meanwhile, the technical performance of the PCD-DSCT has been assessed.[26] In the clinical examples in this review article, we will mostly refer to this clinical system.

PHYSICAL PRINCIPLES OF PHOTON-COUNTING DETECTOR CT

The central element of PCD-CT is a new detector. The detector of a CT system records the x-rays attenuated by the patient. It consists of 16–320 rows of approximately 1000 individual detector pixels and resembles a fast digital x-ray camera.

Photon-counting detectors are made of semiconductors such as CdTe, CZT, or silicon (Si). Because of their high atomic number, the CdTe and CZT layers can be relatively thin (1.4–2 mm) and still provide high x-ray absorption. Photon-counting detectors made of Si need to be much thicker to absorb sufficiently (30–60 mm). According to the current literature, all PCD-CTs in preclinical or clinical use are equipped with CdTe or CZT detectors. The schematic structure of a CdTe- or CZT-based PCD is shown in Figure 1. On the upper side of the semiconductor layer, a large-area cathode electrode is deposited, and on the lower side pixelated anode electrodes. A high voltage of 800–1000 V applied between the cathode and the individual anodes provides a strong electric field. The incident x-rays are absorbed in the semiconductor, creating charges (electron-hole pairs) that are separated in this electric field. The electrons move to the anodes and induce short current pulses there with a duration of about a nanosecond (10^{-9} seconds), which are converted by an electronic pulse shaping circuit into voltage pulses with a half-width (FWHM) of 10–15 nanoseconds. The pulse height of the voltage pulses is proportional to the absorbed energy E of the x-rays. As soon as the pulses exceed a threshold T_L corresponding to an absorbed energy of typically 20–25 keV, they are counted by readout electronics. In the technical realization, a pulse height comparator circuit is used into which a voltage corresponding to the threshold energy is fed, see also Figure 1. The detector signal corresponds to the sum of all pulses registered during the measurement time of a projection.

To obtain spectrally resolved data, multiple counters operating at different threshold energies are read out simultaneously, see Figure 2. The detector then provides a separate data stream for each threshold, containing only those x-ray quanta whose energy exceeds the respective threshold energy, see also Figure 2. The images reconstructed from the data stream containing all x-ray quanta with energies above the lowest threshold energy T_L (T_L images, proprietary for Siemens also called T3D images) are comparable to images obtained with a conventional CT at the same x-ray tube voltage (kVp). However, in realistic PCDs, there are inaccuracies in the energy registration due to unavoidable physical effects that reduce the spectral separation of the signals, such as charge sharing at pixel boundaries or energy loss of the x-ray quanta due to fluorescence. These effects, shown schematically in Figure 3, cause quanta to be erroneously counted twice at x-ray energies that are too low. Silicon PCDs experience less from charge sharing and fluorescence than CdTe-PCDs or CZT-PCDs and therefore have better spectral separation, but most x-ray quanta are primarily scattered in the Si crystal and not directly absorbed; they often leave a detector pixel without contributing to the signal, so the detective quantum efficiency of the detector is reduced, and higher radiation dose is required for all detection tasks.[27] Another challenge for PCDs is pulse pile-up. At very high x-ray flux, the

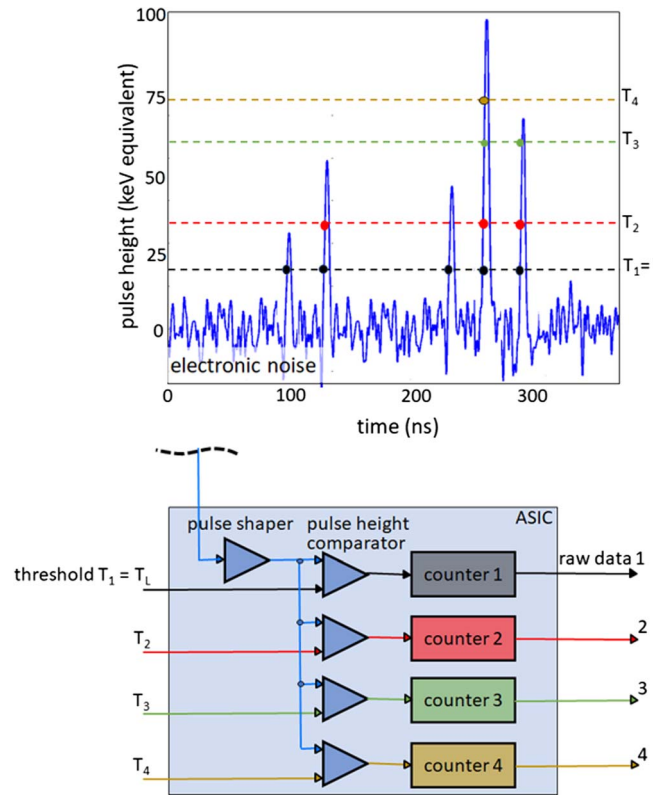

FIGURE 2. Schematic illustration of spectral data acquisition with a PCD. Shown above is a time sequence of voltage pulses generated by absorbed x-ray quanta of various energies. Below, the technical realization of a 4-threshold counter is schematically indicated. In this example, 4 counters operating at 20, 35, 60, and 75 keV threshold energy are read out simultaneously. The detector provides 4 raw data streams containing only counted x-ray quanta with absorbed energy greater than the respective threshold energy.

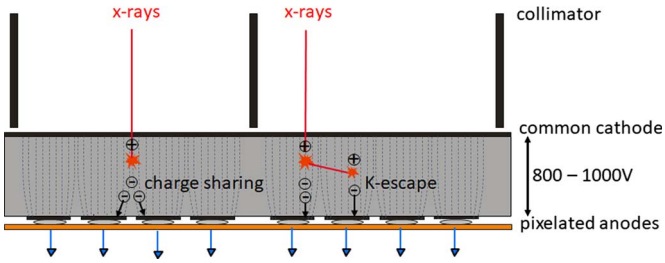

FIGURE 3. Schematic illustration of charge sharing and K-escape that reduce the energy separation of a realistic PCD. X-rays absorbed close to pixel borders produce electrons that generate signals in neighboring pixels (charge sharing). Thus, an x-ray photon is erroneously counted several times with too low energy. Incident x-rays can also initially knock out inner shell electrons from the detector material (K-electrons). This produces fluorescence radiation, which is reabsorbed and counted in the detector cell itself or in neighboring detector cells (K-escape). The incident x-rays at the primary interaction site are counted with too low energy.

generated voltage pulses overlap in time and are no longer counted separately. However, pile-up does not play a role at realistic CT flux rates.

BENEFITS OF PHOTON-COUNTING DETECTOR CT AND THEIR CLINICAL TRANSLATION

Through their detection principle, PCDs have the potential to overcome some of the limitations of conventional energy-integrating scintillation detectors (EIDs), which have been used in virtually all CT equipment so far.

Absence of Electronic Noise

As in any electronic device, there is a certain amount of background noise in the readout electronics of detectors. In PCDs, the lowest threshold energy that x-ray quanta must exceed to be counted is approximately 20 keV; there are no x-rays below this energy in the primary beam of the x-ray tube, because they are removed by a prefilter. This threshold energy is well above the noise floor of electronics, so electronic noise does not affect the count rates of a PCD, see Figure 2. Thus, even at low x-ray flux, the signal shows only the statistical quantum noise of the x-ray photons. In conventional EIDs, on the other hand, electronic noise dominates the signal at low x-ray flux, and as a result, image noise increases sharply, noise streaks appear, and the stability of CT values suffers. Photon-counting detectors provide significantly better, lower-noise images when examining obese patients and for low-dose scans, thus opening up the possibility of reducing the radiation dose even further than today. The superior image quality of PCDs at low radiation doses, particularly due to the lack of electronic noise, was noted early on in preclinical prototypes both in phantom scans[28,29] and in initial studies in volunteers. The focus was on dose-reduced lung imaging,[19] which is important in the context of lung cancer screening, among others. More recently, the potential of PCD-CT to reduce the radiation dose in the assessment of interstitial lung disease (ILD) in systemic sclerosis patients was evaluated. In a study of 80 patients initially scanned with third-generation DSCT, followed by first-generation PCD-DSCT, for follow-up,[30] PCD-CT at a mean $CTDI_{vol}$ of 0.72 mGy was shown to provide comparable image noise, subjective image quality, and diagnostic accuracy as DSCT at 2.3 mGy. The authors concluded that with PCD-CT, a 66% reduction in radiation dose is possible in the evaluation of ILD without compromising diagnostic accuracy. Similar possibilities for dose reduction with comparable or even better image quality were also described by others.[31] Photon-counting detector CT thorax examinations performed at ultra-low radiation dose (mean size-specific dose estimate, 0.45 mGy) in pediatric patients (mean age, 2.6 years) showed good to excellent image quality for lung structures and moderate image quality for soft tissue structures.[32] The potential of PCD-CT in the examination of severely obese patients, who still pose major challenges to CT today, was investigated in a recent study with 51 overweight patients (median body mass index [BMI], 32.15 kg/m^2) who underwent clinically indicated, contrast-enhanced abdominal CT on both second-generation DSCT and first-generation PCD-DSCT.[33] The authors observed significant dose reduction (mean $CTDI_{vol}$ of 12.00 mGy for PCD-CT vs 16.05 mGy for DSCT) while maintaining similar or even improved image quality. The benefits of PCD-CT in the evaluation of obese oncologic patients have also been described elsewhere.[34]

Improved Spatial Resolution by Smaller Detector Pixels

Photon-counting detectors can be more finely structured than conventional EIDs. In EIDs, the individual detector pixels must be separated by opaque intermediate layers to prevent optical crosstalk. These interlayers have a thickness of approximately 0.1 mm and reduce the dose efficiency of the detector because the x-ray quanta absorbed in them do not contribute to the detector signal. The smaller the active detector pixels are structured, the more the relative area of these inactive layers increases and the lower the dose efficiency becomes. Therefore, the detector pixels of EIDs cannot be made significantly smaller than they are today. Alternative techniques for increasing spatial resolution in special applications such as inner ear scanning, which are based on reducing the active areas of the detector pixels by moveable comb apertures, have the disadvantage of significantly increased radiation dose due to substantially decreasing the dose efficiency of the detector.[35]

Photon-counting detectors, on the other hand, do not require interlayers between the individual pixels, see Figure 1. The detector pixels can be much smaller than those of EIDs, resulting in significantly higher spatial resolution. A prerequisite for this is a correspondingly small focal spot of the x-ray tube, even if this comes at the expense of reduced tube power. Otherwise, the focal spot size will limit the spatial resolution. The increased spatial resolution of PCD-CT has already been successfully demonstrated on preclinical prototypes. For example, a spatial resolution of 0.15 mm in the scan plane and slice-width of 0.41 mm was obtained for the hybrid dual-source PCD-CT.[36] The detector pixels of the preclinical prototypes vary in size between 0.225 × 0.225 mm^2 and 0.5 × 0.5 mm^2 depending on the manufacturer; in any case, they are significantly smaller than those of EID-CT systems.

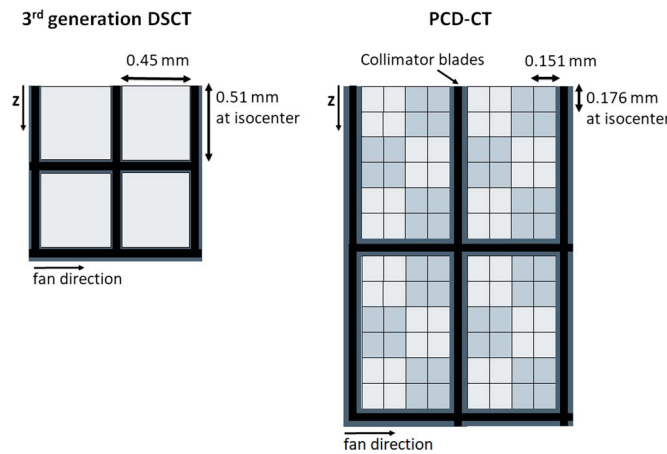

FIGURE 4. Schematic detector structure of a third generation DSCT with a scintillator detector (left) and a commercial PCD-DSCT (right). View from the top, the z-direction is the patient's longitudinal direction. The thick black lines schematically represent the collimator grid to suppress scattered radiation. The detector pixels of the PCD are read out separately in the ultra-high-resolution mode. For standard scanning, 2×2 pixels are combined into 1 macro pixel – this is indicated by light and dark gray squares.

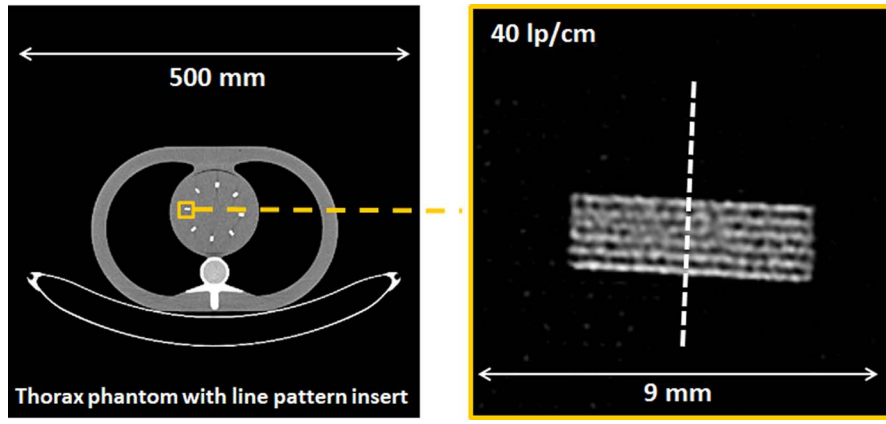

FIGURE 5. Demonstration of 40 lp/cm spatial resolution achieved on a PCD-CT with a detector as schematically shown in Figure 4. For reconstruction, the sharpest kernel Br98 was used. Image courtesy of Matthias Baer-Beck, Siemens Healthineers, Forchheim, Germany.

Figure 4 shows the detector structure of a commercially available PCD-CT, in comparison to a third-generation DSCT. The detector pixels have a size of 0.275 × 0.322 mm^2 (0.151 × 0.176 mm^2 at the isocenter). Each group of 4 × 6 detector pixels is separated from the neighboring groups by a 2-dimensional collimator grid to reduce scattered radiation. With this detector and a focal spot of 0.4 × 0.4 mm^2, a resolution of 40 lp/cm, corresponding to 0.125 mm, can be achieved, see Figure 5; this is about twice as sharp as with EID-CT systems. In CT, increased spatial resolution is always associated with increased image noise or correspondingly increased radiation dose; this basic law of CT also applies to PCD-CT. Refined noise reduction techniques are therefore mandatory, either iterative or deep-learning based.[37]

Clinically, exceptional spatial resolution is essential for evaluating small bony structures such as those in the inner ear or wrist. Advantages can be expected in lung examinations, especially for differential diagnosis of ILD, and in CT angiography of small vessels, for example, in the head and neck region and the extremities. In cCTA, previous limitations due to severe calcification leading to overestimation of stenoses may be overcome. Advantages in the clinical fields mentioned here have already been demonstrated with preclinical prototypes.[36,38–40]

More recently, in a study on 5 cadaveric heads, the authors could show that PCD-CT provides superior image quality and significant dose savings (mean dose reduction of 79.3%) compared with EID-CT for ultra-high-resolution (UHR) examinations of the temporal bone.[41] In temporal bone examinations of 13 patients, PCD-CT was rated superior for the evaluation of all individual anatomic structures at an average 31% lower radiation dose compared with an EID-CT.[42] Figure 6 shows a clinical example illustrating the potential of PCD-CT in inner ear imaging. In a comparison of the visualization of the smallest bone details between PCD-CT and EID-CT using a mouse as a specimen, PCD-CT was found to provide significantly less image noise, higher signal-to-noise ratio, and higher edge sharpness than EID-CT in dose-matched scans.[43] In trabecular bone imaging, the effective volumetric spatial resolution of PCD-CT, defined as the number of separately representable elements per mm^3, was comparable with that of high-resolution peripheral CT and more than 5 times higher compared with conventional CT.[44]

In high-resolution lung imaging, PCD-CT provided better image quality while using significantly less radiation dose compared with EID-CT.[31,45] In a study of 30 patients, who underwent conventional EID-CT and PCD-CT because of suspected ILD, UHR PCD-CT demonstrated significantly better overall image quality and sharpness at a slightly lower radiation dose. Furthermore, it improved the readers' confidence in the presence or absence of imaging findings of reticulation, ground-glass opacities, and mosaic pattern with idiosyncratic improvement in confidence in usual interstitial pneumonia presence,[46] see also the example in Figure 7. A phantom study comparing PCD-CT and EID-CT confirmed more accurate lung nodule volume and airway wall thickness quantification at lower radiation dose for high-resolution PCD-CT.[47]

Coronary CTA is another application that benefits from increased spatial resolution. Despite all technical advances, certain patient groups still have a high-risk of obtaining nondiagnostic image quality; severe

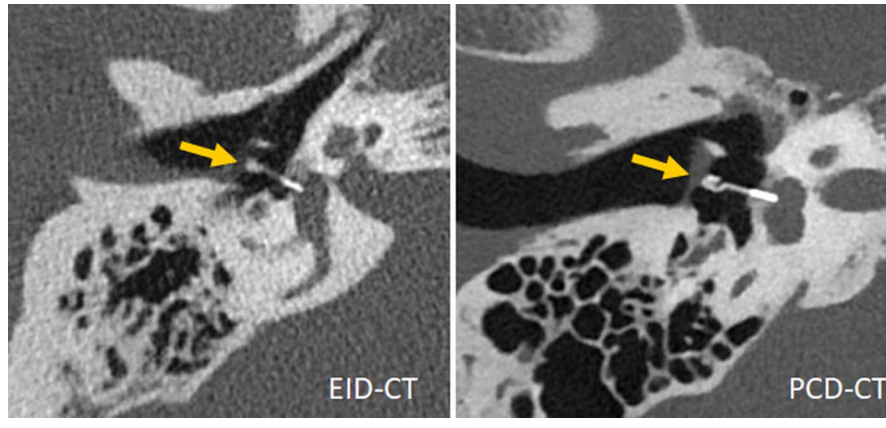

FIGURE 6. Inner ear scans acquired with a third-generation DSCT (left) and a first-generation PCD-DSCT, (right), demonstrating superior visualization of a Titanium K-piston stapes prosthesis (arrow, distal end diameter 0.4 mm) with PCD-CT. Courtesy of Dr A. van der Lugt, Erasmus Medical Center, Rotterdam, the Netherlands.

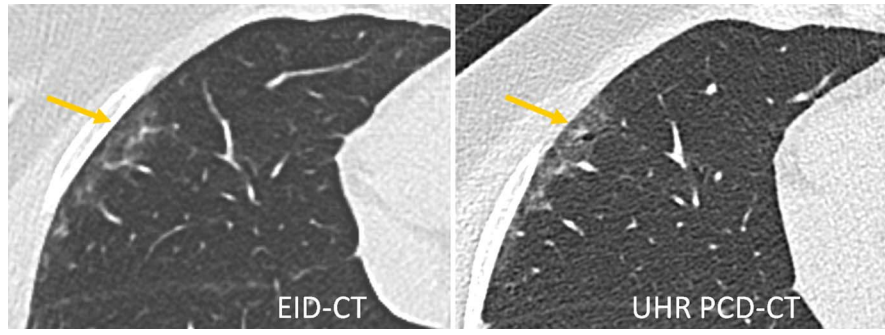

FIGURE 7. Lung scan of a patient with interstitial lung disease acquired with a third-generation DSCT (left) and a first-generation PCD-DSCT, (right). The UHR PCD-CT scan confirms the presence of traction bronchiolectasis in the periphery of the right middle lobe (arrow), superimposed on mild ground-glass attenuation. This finding was missed on the EID-CT scan. Courtesy of Dr Martine Remy-Jardin, Hôpital Calmette, Lille, France.

coronary artery calcifications represent the greatest risk for a nondiagnostic examination.[48] Also, there is only a limited recommendation of cCTA for patients with stents. The very high resolution of PCD-CT can potentially address the current limitations of cCTA, in particular, the problem of overestimation of stenoses in the presence of strong calcifications and calcium blooming. In a motion phantom study, improved stenosis quantification accuracy and reduced blooming artifacts were demonstrated with UHR PCD-DSCT compared with standard resolution CT, independent of the heart rate.[49] In a study with 14 participants undergoing cCTA on dual layer EID-CT and a prototype PCD-CT, the scores for overall image quality and diagnostic confidence were higher with PCD-CT images for 100%, 92%, and 45% of the coronary calcification, stent, and noncalcified plaque cases, respectively.[22] In a study with 20 patients[50] on a PCD-DSCT, UHR cCTA with 0.2-mm slice width and image reconstruction with a sharp kernel (Bv64 or Bv72) provided excellent anatomic visualization of plaques and the surrounding vessel lumen with no perceived blooming. In a quantitative evaluation, blooming artifacts decreased from 52.8% with a standard medium-sharp kernel (Bv40) to 39.7% with Bv72. Ultra-high-resolution PCD-CT resulted in significant differences in quantitative coronary plaque characterization.[51] In 22 plaques of 20 patients, total plaque volume and volume of calcified components were on average 23% and 32% lower on reconstructions with a slice thickness of 0.2 mm and the Bv64 kernel compared with the reference standard. The volume of fibrous components remained similar, whereas that of lipid components increased significantly. In a coronary CTA of a 68-year-old patient presenting with chest pain, UHR PCD-DSCT could visualize microcalcifications and fibrous caps, which optical coherence tomography confirmed.[52] Figure 8 shows an example of a coronary plaque both in a standard and in a UHR reconstruction.

Improved Iodine Contrast-to-Noise Ratio

In EIDs, absorbed x-ray quanta with low x-ray energy produce less light than those with high energy, and they, therefore, contribute less to the detector signal. An EID generates a signal corresponding to the total x-ray energy registered during the measurement time of a projection. Photon-counting detectors, on the other hand, count all x-ray quanta whose energy exceeds the lowest energy threshold with equal weight. Low-energy x-ray quanta contribute as much to the detector signal as higher-energy x-rays. Most low-contrast information is contained in the low x-ray energy range, so low-contrast differences tend to be more pronounced in PCD-CT. This is especially true for CT scans with iodinated contrast agents. Iodine has a K-edge at 33 keV; it absorbs most strongly in the low-energy region just above the K-edge. In PCD-CT images, the iodine contrast is therefore higher than in EID-CT images acquired with the same x-ray tube voltage (kVp). The difference is more pronounced the higher the x-ray tube voltage is.[53] The higher iodine signal results in a higher iodine contrast-to-noise ratio (CNR) at the same radiation dose. In a study on a preclinical PCD-CT prototype using 4 anthropomorphic phantoms of different sizes,[53] a mean increase in iodine CNR of 11%, 23%, 31%, and 38% was observed at 80, 100, 120, and 140 kVp, respectively.

Clinically, increased iodine CNR translates into better image quality in contrast-enhanced scans or a potential reduction of radiation or contrast agent dose. In an early phantom study, a dose reduction of 32% thanks to higher iodine CNR was realized.[54] In an oncological cohort of 70 patients who underwent routine contrast-enhanced abdominal and pelvic CT first on a second-generation DSCT and for follow-up on PCD-CT,[55] similar or even better image quality (higher liver lesion conspicuity) was observed for the T_L images of the PCD-CT at a mean radiation dose

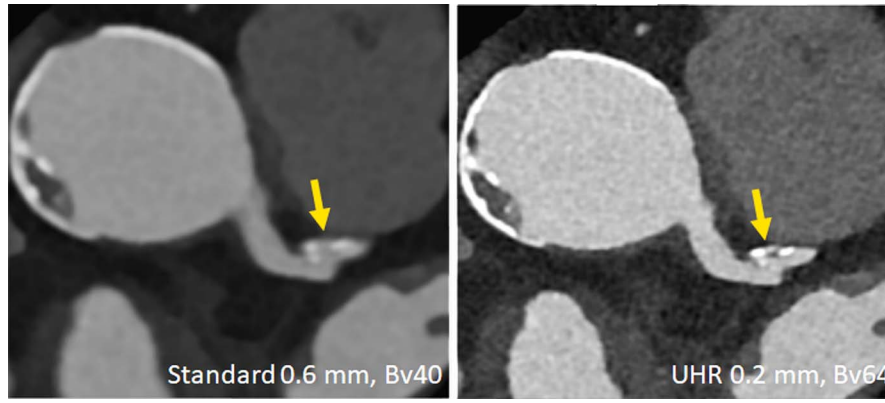

FIGURE 8. Clinical example demonstrating improved characterization of coronary plaques with UHR PCD-CT. A plaque that appears essentially calcified in a standard reconstruction (left) turns out to be mixed and smaller in volume in the UHR image (right). Image courtesy of Drs V. Mergen and H. Alkadhi, University Hospital Zurich, Switzerland.

reduction of 32% compared with DSCT (mean $CTDI_{vol}$/DLP = 7.98 mGy/393.1 mGy × cm for PCD-CT and 14.11 mGy/693.6 mGy × cm for DSCT). The authors attributed this result, which is well in line with,[54] to the improved weighting of low-energy x-ray quanta leading to higher iodine contrast, aided by the absence of electronic noise and improved iterative reconstruction. In a similar study of 100 oncologic chest patients,[56] a mean radiation dose reduction of more than 40% at maintained image quality compared with second-generation DSCT was demonstrated (mean $CTDI_{vol}$/DLP = 4.17 mGy/151.0 mGy × cm for PCD-CT and 7.21 mGy/288.6 mGy × cm for DSCT).

Spectral Imaging Capabilities

In multithreshold mode, a PCD simultaneously provides multiple detector signals containing only x-ray quanta with energies greater than the corresponding energy threshold, see Figure 1. With 2 energy thresholds, all currently established dual-energy applications are possible, which are based on a material decomposition into 2 base materials such as iodine and water. Thus, virtual monoenergetic images (VMIs), iodine maps, or virtual noncontrast (VNC) images can be routinely calculated in any patient examination where these results might be relevant. Virtual noncontrast is another term for the soft tissue image after material decomposition into iodine and soft tissue fractions. Virtual monoenergetic images are based on the same material decomposition. Here, however, the base material images are scaled so that the attenuation of the iodine and the soft tissue is exactly as if the images were acquired with monoenergetic x-rays of the desired energy (in keV) and recombined to the VMI. For other materials, such as, for example, Ca, the attenuation at the desired keV is not correctly reproduced.

The first-generation clinical PCD-CT has implemented an approach to provide a standardized acquisition protocol at 120 kVp or 140 kVp for all routine contrast-enhanced examinations. Similar approaches have been proposed for abdominal CT examinations in all patient sizes.[57,58] The primary image output of each CT scan is VMIs at a keV level tailored to the clinical question, which is, for example, 60–65 keV for imaging parenchymal organs, or 45–55 keV for CT angiography. The iodine CNR of the VMIs is improved by refined algorithms[59] such that it increases with decreasing keV similarly as if the images were acquired with lower tube voltage (kVp), see Figure 9. This approach achieves a better standardization of CT image results[60] because the iodine contrast in VMIs only depends on the selected keV level and is independent of their acquisition conditions, especially the x-ray tube voltage.

Several clinical studies have investigated the image quality of VMIs from PCD-CT, their CNR, and the associated radiation dose to the patient compared with EID-CT.[61] A cohort of 50 oncologic patients with liver metastases scanned with a PCD-CT at 120 kV was compared with a matched group of 50 patients scanned with an EID-CT with automatic tube voltage selection, proposing 100 kV for most of the scans.[34] Compared with the polychromatic images from EID-CT, the VMIs from PCD-CT demonstrated reduced image noise at 70 keV and consistently higher CNR in the 40–70 keV range at a similar radiation dose ($CTDI_{vol}$ of 6.7 mGy for PCD-CT vs 6.4 mGy for EID-CT). Furthermore, the conspicuity of hypovascularized liver metastases was significantly higher at low keV, and patients with high BMI benefitted from PCD-CT as the image noise and lesion conspicuity were preserved compared with low BMI patients. In another study,[62] 40 patients underwent CTA of the thoracoabdominal aorta on a third-generation DSCT in the high-pitch mode. The optimal tube voltage was selected by automatic tube voltage selection (reference voltage, 100 kV). Each patient received a follow-up scan at matched radiation dose on a PCD-CT with 120 kV tube voltage, and VMIs were reconstructed at 40, 45, 50, and 55 keV. The mean CNR was significantly higher for 40 and 45 keV of PCD-CT as compared with the EID-CT images, with the CNR gain increasing in overweight patients. In a subjective image analysis considering the increased image noise at 40 and 45 keV, VMIs at 45 to 50 keV were found to be the best compromise. The tendency for iodine CNR to be highest at very low keV (eg, 40 keV) but for slightly higher keV (eg, 50 keV) to be preferred for diagnosis because of the high image noise at 40 keV has also been observed in other studies. In a comparative study of 39 patients undergoing contrast-enhanced abdominal PCD-CT in the portal-venous phase,[63] the authors found optimal results with standardized reconstructions of VMIs at 50 keV, which showed significantly higher CNR at the same radiation dose with similar subjective image quality compared with EID-CT. Figure 10 shows a clinical example of an abdominal CT scan. In PCD-CT examinations of 80 patients with suspected pulmonary embolism (PE), subjective PE visibility was rated highest in VMIs at 50 keV.[64] For coronary CTA, VMIs at 40 keV were preferred when combined with high levels of iterative reconstruction (QIR 3 and QIR 4) both in a phantom evaluation and in a study of 10 patients.[65]

Meanwhile, the possibility of contrast agent reduction when using VMIs at low energy has been investigated. In a dynamic circulation phantom in a PCD-CT diagnostically sufficient iodine CNR was achieved in VMIs reconstructed at 40 keV in coronary CTA even with a 50% reduction in contrast agent concentration.[66] In a group of 60 patients, a protocol with a 25% reduction in contrast agent volume (from 70 mL of a 370 mg I/mL contrast agent in a triphasic protocol to 52.5 mL of the same contrast agent) demonstrated noninferior quality for CTA of the aorta with PCD-CT compared with EID-CT at the same radiation dose, when 50 keV VMIs were used as the best compromise between objective and subjective image quality.[67]

The ability to reconstruct VMIs at different energies may increase diagnosticconfidence. When using VMIs at 50 keV for coronary CTA with a PCD-DSCT at high pitch, a low contrast dose protocol (30 mL of a 350 mg I/mL contrast agent instead of the routine 60 mL) produced diagnostic image quality in a group of 27 patients. The addition of 100 keV

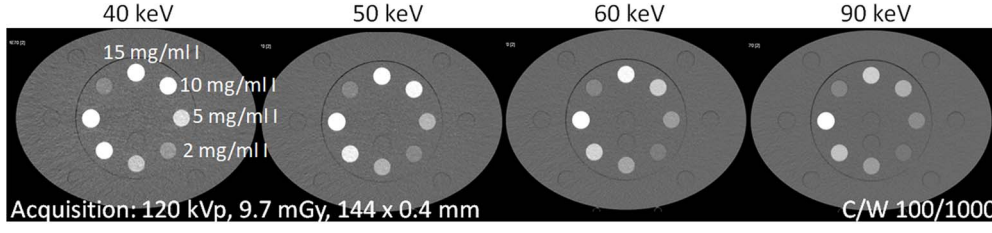

	40 keV	50 keV	60 keV	70 keV	90keV	120 kV T_L image	90 kV T_L image
CNR (15 mg/ml I)	35.7	29.8	23.4	19.8	11.0	21.1	26.5

FIGURE 9. CNR of a tube filled with a 15 mg I/mL solution inserted into the large (40 × 30 cm) Gammex multienergy CT phantom (Sun Nuclear Corporation, Melbourne, FL), scanned with a PCD-DSCT. With decreasing keV level of the VMIs, the iodine CNR increases. The iodine CNR in 55 keV VMIs from a 120 kV scan (interpolated) is equivalent to 90 kV scanning (T_L image at 90 kV), and that in 55 keV VMIs is equivalent to 120 kV scanning.

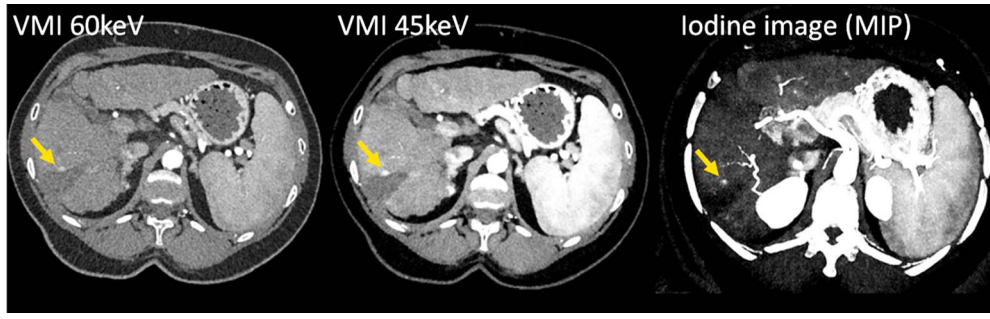

FIGURE 10. CT images of a patient with liver cirrhosis and tumor recurrence after ablation, scanned with a PCD-DSCT (120 kV, 144 × 0.4 mm, $CTDI_{vol}$ = 4.8 mGy). With decreasing keV level of the VMIs (left and center), the iodine CNR increases, and the tumor recurrence (arrow) becomes more evident. The iodine image (right) enables quantification of the iodine uptake. Courtesy of Dr A. van der Lugt, Erasmus Medical Center, Rotterdam, the Netherlands.

VMIs improved the diagnostic confidence in the evaluation of luminal stenosis associated with calcific plaques and stents and downgraded CAD-RADS scores in 9 patients by reducing blooming artifacts.[68]

Virtual monoenergetic images are also used in CT scans without contrast agent, in which case special attention must be paid to the choice of keV level for quantitative applications such as Ca scoring. By choosing an appropriate combination of keV and strength of iterative reconstruction (Quantum Iterative Reconstruction QIR, Siemens Healthcare), Ca scoring results of EID-CT can be reproduced on PCD-CT. In a combined phantom and patient study,[69] the authors demonstrated accurate coronary Ca scoring from 120 kV PCD-DSCT scans using VMIs at 70 keV and QIR0, or 65 keV and QIR3 or QIR4. Image reconstructions with 65 keV and QIR3 at 90 kV and with 70 keV and QIR1 at Sn100kV provided Ca scoring results comparable to EID-CT with the possibility of substantial radiation dose reduction.[70] Accuracy and reproducibility of Ca scoring with PCD-DSCT have also been investigated in other phantom studies.[71,72]

Virtual noncontrast images are of clinical interest because, if of sufficient quality, they may eliminate the need for a nonenhanced CT scan, thus reducing the overall radiation dose to the patient. The image quality of VNC images from PCD-CT has been investigated in several studies, with some controversial findings that may result from early software and scanner versions. A mean absolute error of 4.1 HU was observed in the VNC images of an anthropomorphic abdominal phantom with an iodinated liver insert (1.4 mg I/mL) and 19 liver lesions (iodine content, 0–5 mg/mL).[73] The error was significantly smaller than with EID-CT (third-generation DSCT). The phantom result was

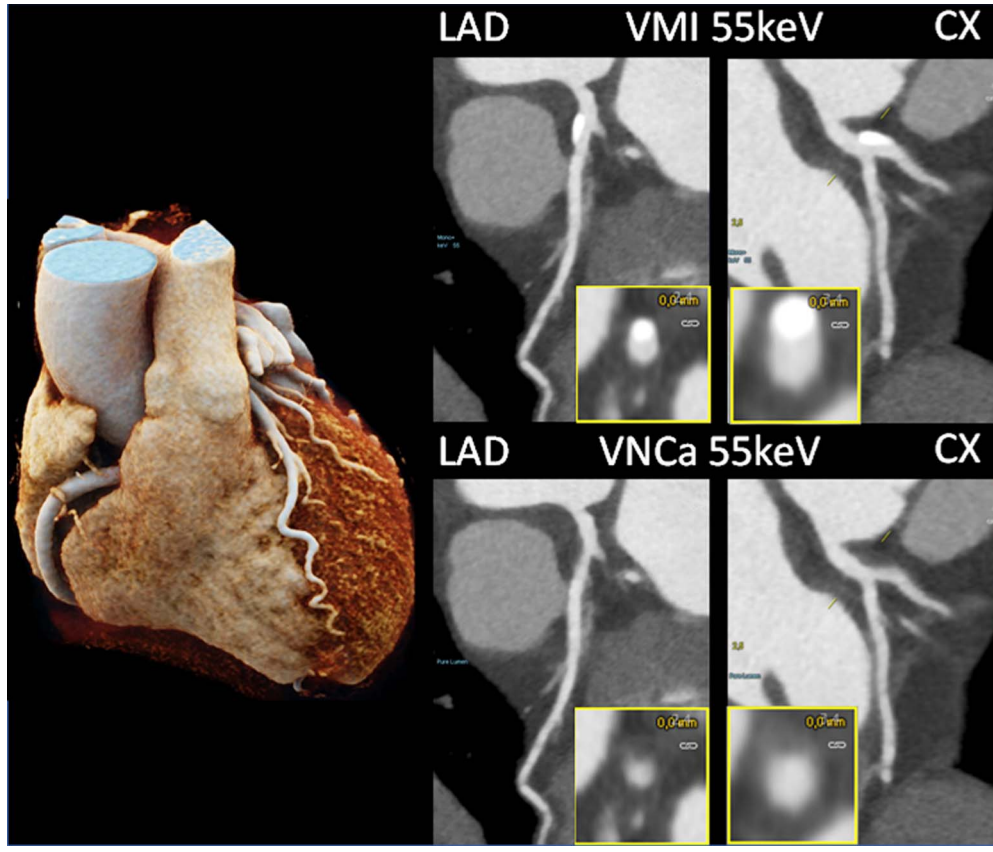

FIGURE 11. Coronary CTA images of a patient with calcifications in the LAD and CX, scanned with a PCD-DSCT (120 kV, 144 × 0.4 mm, 0.25 seconds rotation time, 66 milliseconds temporal resolution). The calcifications shown in the 55 keV VMIs (top) are removed in the 55 keV virtual noncalcium images (bottom). Courtesy of Dr H. Alkadhi, University Hospital Zurich, Switzerland.

confirmed in 15 patients with hypodense liver lesions who had a mean error of 3.7 HU in the VNC images compared with TNC images. In a cohort of 100 patients,[74] abdominal VNC images from the arterial and portal venous phase of PCD-CT yielded accurate CT attenuation and good image quality compared with TNC images, with errors less than 5 HU in 76% and less than 10 HU in 95% of measurements. Subjective image quality was rated lower in VNC images; however, diagnostic quality was reached in 99%–100% of patients. Other studies tended to show larger discrepancies between VNC and TNC,[75] and VNC images from PCD-CT resulted in overestimation and underestimation of the true unenhanced attenuation of adrenal adenomas.[76] When investigating possible clinical applications, VNC images from PCD-CT were found to be reliable for the assessment of hepatic steatosis[77] and for emphysema quantification from contrast-enhanced lung scans.[78]

The combination of high temporal and spatial resolution with spectral data acquisition enables novel applications for cardiovascular CT. For example, material decomposition into iodine and calcium can be used to remove the iodine from cCTAs, leaving only the calcium in the coronary arteries (PURE Calcium, Siemens Healthcare). Unlike the common material decomposition into iodine and soft tissue (VNC images), where calcium splits between both base material images and therefore has a reduced density in the VNC images, this special material decomposition is designed to preserve the Ca density in the PURE Calcium images so that they can potentially be used for Ca scoring. A study with 67 patients[79] demonstrated a high correlation with TNC images but still underestimated the Ca score derived from PURE Calcium images. In comparison, the Ca score from VNC images showed a substantially larger underestimation.

In a related application, also based on material decomposition into iodine and calcium, calcified plaques are removed from the contrast-filled vessels imaged in CTA to provide virtual noncalcium images (PURE Lumen, Siemens Healthcare). A phantom study[80] demonstrated decreased blooming artifacts caused by heavily calcified plaques and improved image interpretability at simulated heart rates of up to 80 beats per minute. This application may therefore allow a better assessment of the vessel lumen; however, its efficacy has to be proven in clinical studies. Figure 11 shows a clinical example. An overview of the potential of PCD-CT for cardiac and myocardial characterization can be found in Zsarnóczay et al,[81] and the applications of the PURE Calcium and PURE Lumen techniques for vascular imaging are demonstrated in Wildberger and Alkadhi.[82]

If more than 2 energy thresholds are implemented, such as the 4 in Figure 2, more than 2 base materials can in principle be separated. For example, one can choose iodine and water as base materials, as before, and separate a third material from these 2 materials. However, this only works if this third material has a K-edge in the relevant CT energy range between 40 and 100 keV. Unfortunately, all elements naturally occurring in the human body do not have K-edges in this range, because their atomic number is too low. Therefore, elements with a high atomic number, such as gadolinium, gold, hafnium, or tungsten, must be introduced into the body as contrast agents to enable multimaterial decomposition. Such applications are the subject of preclinical research.[83–85]

OUTLOOK

To establish PCD-CTs broadly in clinical routine, demonstrating their technical capabilities is not enough. Instead, they must be shown to have a positive impact on diagnostic accuracy and diagnostic confidence, and ideally to change the clinical management of patients. Initial studies already show an impact on diagnostic performance and diagnostic accuracy in various clinical fields,[46,68,77,86,87] and larger, more comprehensive clinical studies are sure to follow.

Furthermore, we are likely to see the great wealth of information in the high-resolution spectral PCD-CT data being exploited even better with refined image analysis, for example, based on radiomics and deep learning. Initial studies have already been initiated here. For example, it has been investigated whether PCD-CT might not allow the detection of textural changes in periaortic adipose tissue in relation to the presence of local aortic calcification because of its better spatial resolution and signal-to-noise ratio, and thus possibly provide a biomarker for the development of atherosclerosis.[88] The stability of radiomics features in abdominal VMIs[89] and in the myocardium[90] has been investigated, and it could be shown that some texture alterations of the left ventricular myocardium might be associated with the severity of coronary artery calcification estimated by the Agatston score.[91] We are here only at the beginning of a development whose real potential will become apparent in further studies.

REFERENCES

1. Andreini D, Mushtaq S, Pontone G, et al. CT perfusion versus coronary CT angiography in patients with suspected in-stent restenosis or CAD progression. *JACC Cardiovasc Imaging*. 2020;13:732–742.
2. Nadarevic T, Giljaca V, Colli A, et al. Computed tomography for the diagnosis of hepatocellular carcinoma in adults with chronic liver disease. *Cochrane Database Syst Rev*. 2021;10:CD013362.
3. Mettler FA Jr., Mahesh M, Bhargavan-Chatfield M, et al. Patient exposure from radiologic and nuclear medicine procedures in the United States: procedure volume and effective dose for the period 2006–2016. *Radiology*. 2020;295:418–427.
4. Taguchi K. Energy-sensitive photon counting detector-based x-ray, computed tomography. *Radiol Phys Technol*. 2017;10:8–22.
5. Willemink MJ, Persson M, Pourmorteza A, et al. Photon-counting CT: technical principles and clinical prospects. *Radiology*. 2018;289:293–312.
6. Leng S, Bruesewitz M, Tao S, et al. Photon-counting detector CT: system design and clinical applications of an emerging technology. *Radiographics*. 2019;39:729–743.
7. Flohr T, Petersilka M, Henning A, et al. Photon-counting CT review. *Phys Med*. 2020;79:126–136.
8. Nakamura Y, Higaki T, Kondo S, et al. An introduction to photon-counting detector CT (PCD CT) for radiologists. *Jpn J Radiol*. 2023;41:266–282.
9. Esquivel A, Ferrero A, Mileto A, et al. Photon-counting detector CT: key points radiologists should know. *Korean J Radiol*. 2022;23:854–865.
10. Tortora M, Gemini L, D'Iglio I, et al. Spectral photon-counting computed tomography: a review on technical principles and clinical applications. *J Imaging*. 2022;8:112.
11. Wehrse E, Klein L, Rotkopf LT, et al. Photon-counting detectors in computed tomography: from quantum physics to clinical practice. *Radiologe*. 2021;61(Suppl 1):1–10.
12. Danielsson M, Persson M, Sjölin M. Photon-counting x-ray detectors for CT. *Phys Med Biol*. 2021;66:03TR01.
13. Sartoretti T, Wildberger JE, Flohr T, et al. Photon-counting detector CT: early clinical experience review. *Br J Radiol*. 2023;20220544.
14. Forghani R, De Man B, Gupta R. Dual-energy computed tomography: physical principles, approaches to scanning, usage, and implementation: part 1. *Neuroimaging Clin N Am*. 2017;27:371–384.
15. Kappler S, Henning A, Kreisler B, et al. Photon-counting CT at elevated x-ray tube currents: contrast stability, image noise and multi-energy performance. *Medical Imaging*. 2014;90331C.
16. Yu Z, Leng S, Jorgensen SM, et al. Evaluation of conventional imaging performance in a research whole-body CT system with a photon-counting detector array. *Phys Med Biol*. 2016;61:1572–1595.
17. Pourmorteza A, Symons R, Sandfort V, et al. Abdominal imaging with contrast-enhanced photon-counting, CT: first human experience. *Radiology*. 2016;279:239–245.
18. Pourmorteza A, Symons R, Reich DS, et al. Photon-counting CT of the brain: in vivo human results and image-quality assessment. *AJNR Am J Neuroradiol*. 2017;38:2257–2263.
19. Symons R, Pourmorteza A, Sandfort V, et al. Feasibility of dose-reduced chest CT with photon-counting detectors: initial results in humans. *Radiology*. 2017;285:980–989.
20. Si-Mohamed S, Boussel L, Douek P. Clinical perspectives of spectral photon-counting CT. In: *Spectral, Photon Counting Computed Tomography: Technology and Applications* vol. 97. Boca Raton, FL: CRC Press; 2020.
21. Boccalini S, Si-Mohamed S, Dessouky R, et al. Feasibility of human vascular imaging of the neck with a large field-of-view spectral photon-counting CT system. *Diagn Interv Imaging*. 2021;102:329–332.
22. Si-Mohamed SA, Boccalini S, Lacombe H, et al. Coronary CT angiography with photon-counting CT: first-in-human results. *Radiology*. 2022;303:303–313.
23. Boccalini S, Si-Mohamed SA, Lacombe H, et al. First in-human results of computed tomography angiography for coronary stent assessment with a spectral photon counting computed tomography. *Invest Radiol*. 2022;57:212–221.

24. Si-Mohamed SA, Boccalini S, Villien M, et al. First experience with a whole-body spectral photon-counting CT clinical prototype. *Invest Radiol*. 2023. doi:10.1097/RLI.0000000000000965.
25. Ferda J, Vendiš T, Flohr T, et al. Computed tomography with a full FOV photon-counting detector in a clinical setting, the first experience. *Eur J Radiol*. 2021;137:109614.
26. Rajendran K, Petersilka M, Henning A, et al. First clinical photon-counting detector CT system: technical evaluation. *Radiology*. 2022;303:130–138.
27. Persson M, Wang A, Pelc NJ. Detective quantum efficiency of photon-counting CdTe and Si detectors for computed tomography: a simulation study. *J Med Imaging (Bellingham)*. 2020;7:043501.
28. Yu Z, Leng S, Kappler S, et al. Noise performance of low-dose CT comparison between an energy integrating detector and a photon-counting detector using a whole-body research photon-counting CT scanner. *J Med Imaging (Bellingham)*. 2016;3:043503.
29. Symons R, Cork TE, Sahbaee P, et al. Low-dose lung cancer screening with photon-counting CT: a feasibility study. *Phys Med Biol*. 2017;62:202–213.
30. Jungblut L, Euler A, von Spiczak J, et al. Potential of photon-counting detector CT for radiation dose reduction for the assessment of interstitial lung disease in patients with systemic sclerosis. *Invest Radiol*. 2022;57:773–779.
31. Graafen D, Emrich T, Halfmann MC, et al. Dose reduction and image quality in photon-counting detector high-resolution computed tomography of the chest: routine clinical data. *J Thorac Imaging*. 2022;37:315–322.
32. Tsiflikas I, Thater G, Ayx I, et al. Low dose pediatric chest computed tomography on a photon counting detector system—initial clinical experience. *Pediatr Radiol*. 2023. doi:10.1007/s00247-022-05584-4.
33. Hagen F, Hofmann J, Wrazidlo R, et al. Image quality and dose exposure of contrast-enhanced abdominal CT on a 1st generation clinical dual-source photon-counting, detector CT in obese patients vs. a 2nd generation dual-source dual energy integrating detector CT. *Eur J Radiol*. 2022;151:110325.
34. Bette S, Decker JA, Braun FM, et al. Optimal conspicuity of liver metastases in virtual monochromatic imaging reconstructions on a novel photon-counting detector CT-effect of keV settings and BMI. *Diagnostics (Basel)*. 2022;12:1231.
35. Flohr TG, Stierstorfer K, Süss C, et al. Novel ultrahigh resolution data acquisition and image reconstruction for multi-detector row CT. *Med Phys*. 2007;34:1712–1723.
36. Leng S, Rajendran K, Gong H, et al. 150-µm spatial resolution using photon-counting detector computed tomography technology: technical performance and first patient images. *Invest Radiol*. 2018;53:655–662.
37. Huber NR, Ferrero A, Rajendran K, et al. Dedicated convolutional neural network for noise reduction in ultra-high-resolution photon-counting detector computed tomography. *Phys Med Biol*. 2022;67:10.1088/1361-6560/ac8866.
38. Zhou W, Lane JI, Carlson ML, et al. Comparison of a photon-counting-detector CT with an energy-integrating-detector CT for temporal bone imaging: a cadaveric study. *AJNR Am J Neuroradiol*. 2018;39:1733–1738.
39. Bartlett DJ, Koo CW, Bartholmai BJ, et al. High-resolution chest computed tomography imaging of the lungs: impact of 1024 matrix reconstruction and photon-counting detector computed tomography. *Invest Radiol*. 2019;54:129–137.
40. Bratke G, Hickethier T, Bar-Ness D, et al. Spectral photon-counting computed tomography for coronary stent imaging: evaluation of the potential clinical impact for the delineation of in-stent restenosis. *Invest Radiol*. 2020;55:61–67.
41. Grunz JP, Heidenreich JF, Lennartz S, et al. Spectral shaping via tin prefiltration in ultra-high-resolution photon-counting and energy-integrating detector CT of the temporal bone. *Invest Radiol*. 2022;57:819–825.
42. Benson JC, Rajendran K, Lane JI, et al. A new frontier in temporal bone imaging: photon-counting detector CT demonstrates superior visualization of critical anatomic structures at reduced radiation dose. *AJNR Am J Neuroradiol*. 2022;43:579–584.
43. Bette SJ, Braun FM, Haerting M, et al. Visualization of bone details in a novel photon-counting dual-source, CT scanner-comparison with energy-integrating CT. *Eur Radiol*. 2022;32:2930–2936.
44. Thomsen FSL, Horstmeier S, Niehoff JH, et al. Effective spatial resolution of photon counting CT for imaging of trabecular structures is superior to conventional clinical CT and similar to high resolution peripheral CT. *Invest Radiol*. 2022;57:620–626.
45. Woeltjen MM, Niehoff JH, Michael AE, et al. Low-dose high-resolution photon-counting, CT of the lung: radiation dose and image quality in the clinical routine. *Diagnostics (Basel)*. 2022;12:1441.
46. Inoue A, Johnson TF, White D, et al. Estimating the clinical impact of photon-counting-detector CT in diagnosing usual interstitial pneumonia. *Invest Radiol*. 2022;57:734–741.
47. Dunning CAS, Marsh JF Jr., Winfree T, et al. Accuracy of nodule volume and airway wall thickness measurement using low-dose chest CT on a photon-counting detector CT scanner. *Invest Radiol*. 2023;58:283–292.
48. Vanhecke TE, Madder RD, Weber JE, et al. Development and validation of a predictive screening tool for uninterpretable coronary CT angiography results. *Circ Cardiovasc Imaging*. 2011;4:490–497.
49. Zsarnoczay E, Fink N, Schoepf UJ, et al. Ultra-high resolution photon-counting coronary CT angiography improves coronary stenosis quantification over a wide range of heart rates—a dynamic phantom study. *Eur J Radiol*. 2023;161:110746.
50. Mergen V, Sartoretti T, Baer-Beck M, et al. Ultra-high-resolution coronary CT angiography with photon-counting detector CT: feasibility and image characterization. *Invest Radiol*. 2022;57:780–788.
51. Mergen V, Eberhard M, Manka R, et al. First in-human quantitative plaque characterization with ultra-high resolution coronary photon-counting CT angiography. *Front Cardiovasc Med*. 2022;9:981012.
52. Emrich T, Hell M. Plaque composition on ultra-high-resolution coronary computed tomography angiography with optical coherence tomography correlation. *Eur Heart J*. 2022;ehac560.
53. Gutjahr R, Halaweish AF, Yu Z, et al. Human imaging with photon counting-based computed tomography at clinical dose levels: contrast-to-noise ratio and cadaver studies. *Invest Radiol*. 2016;51:421–429.
54. Kappler S, Hannemann T, Kraft E, et al. First results from a hybrid prototype CT scanner for exploring benefits of quantum-counting in clinical CT. In: Pelc NJ, Nishikawa RM, Whiting BR, eds. *Medical Imaging 2012: Physics of Medical Imaging; 83130X*. New York, NY: SPIE; 2012.
55. Wrazidlo R, Walder L, Estler A, et al. Radiation dose reduction in contrast-enhanced abdominal CT: comparison of photon-counting detector CT with 2nd generation dual-source dual-energy, CT in an oncologic cohort. *Acad Radiol*. 2022;S1076-6332(22)00324-5. doi:10.1016/j.acra.2022.05.021.
56. Hagen F, Walder L, Fritz J, et al. Image quality and radiation dose of contrast-enhanced chest-CT, acquired on a clinical photon-counting detector CT vs. second-generation dual-source, CT in an oncologic cohort: preliminary results. *Tomography*. 2022;8:1466–1476.
57. Zhou W, Abdurakhimova D, Bruesewitz M, et al. Impact of photon counting detector technology on kV selection and diagnostic workflow in CT. Proc SPIE Int Soc Opt Eng 2018;10573. pii: 105731C
58. Zhou W, Michalak GJ, Weaver JM, et al. A universal protocol for abdominal CT examinations performed on a photon-counting detector CT system: a feasibility study. *Invest Radiol*. 2020;55:226–232.
59. Grant KL, Flohr TG, Krauss B, et al. Assessment of an advanced image-based technique to calculate virtual monoenergetic computed tomographic images from a dual-energy examination to improve contrast-to-noise ratio in examinations using iodinated contrast media. *Invest Radiol*. 2014;49:586–592.
60. McCollough CH, Rajendran K, Leng S. Standardization and quantitative imaging with photon-counting detector CT. *Invest Radiol*. 2023. doi:10.1097/RLI.0000000000000948.
61. Schwartz FR, Samei E, Marin D. Exploiting the potential of photon-counting CT in abdominal imaging. *Invest Radiol*. 2023. doi:10.1097/RLI.0000000000000949.
62. Euler A, Higashigaito K, Mergen V, et al. High-pitch photon-counting detector computed tomography angiography of the aorta: intraindividual comparison to energy-integrating detector computed tomography at equal radiation dose. *Invest Radiol*. 2022;57:115–121.
63. Higashigaito K, Euler A, Eberhard M, et al. Contrast-enhanced abdominal CT with clinical photon-counting detector CT: assessment of image quality and comparison with energy-integrating detector CT. *Acad Radiol*. 2022;29:689–697.
64. Yalynska T, Polacin M, Frauenfelder T, et al. Impact of photon counting detector CT derived virtual monoenergetic images on the diagnosis of pulmonary embolism. *Diagnostics (Basel)*. 2022;12:2715.
65. Sartoretti T, McDermott M, Mergen V, et al. Photon-counting detector coronary CT angiography: impact of virtual monoenergetic imaging and iterative reconstruction on image quality. *Br J Radiol*. 2023;96:20220466.
66. Emrich T, O'Doherty J, Schoepf UJ, et al. Reduced iodinated contrast media administration in coronary CT angiography on a clinical photon-counting detector CT system: a phantom study using a dynamic circulation model. *Invest Radiol*. 2022;58:148–155.
67. Higashigaito K, Mergen V, Eberhard M, et al. CT angiography of the aorta using photon-counting detector CT with reduced contrast media volume. *Radiol Cardiothorac Imaging*. 2023;5:e220140.
68. Rajiah PS, Dunning CAS, Rajendran K, et al. High-pitch multienergy coronary CT angiography in dual-source photon-counting, detector CT scanner at low iodinated contrast dose. *Invest Radiol*. 2023. doi:10.1097/RLI.0000000000000961.
69. Eberhard M, Mergen V, Higashigaito K, et al. Coronary calcium scoring with first generation dual-source photon-counting, CT-first evidence from phantom and in-vivo scans. *Diagnostics (Basel)*. 2021;11:1708.
70. Mergen V, Higashigaito K, Allmendinger T, et al. Tube voltage-independent coronary calcium scoring on a first-generation dual-source, photon-counting CT—a proof-of-principle phantom study. *Int J Cardiovasc Imaging*. 2021. doi:10.1007/s10554-021-02466-y.

71. van der Werf NR, Booij R, Greuter MJW, et al. Reproducibility of coronary artery calcium quantification on dual-source CT and dual-source photon-counting, CT: a dynamic phantom study. *Int J Cardiovasc Imaging*. 2022. doi:10.1007/s10554-022-02540-z.
72. van der Werf NR, Greuter MJW, Booij R, et al. Coronary calcium scores on dual-source photon-counting, computed tomography: an adapted Agatston methodology aimed at radiation dose reduction. *Eur Radiol*. 2022;32:5201–5209.
73. Sartoretti T, Mergen V, Higashigaito K, et al. Virtual noncontrast imaging of the liver using photon-counting detector computed tomography: a systematic phantom and patient study. *Invest Radiol*. 2022;57:488–493.
74. Mergen V, Racine D, Jungblut L, et al. Virtual noncontrast abdominal imaging with photon-counting detector CT. *Radiology*. 2022;305:107–115.
75. Niehoff JH, Woeltjen MM, Laukamp KR, et al. Virtual non-contrast versus true non-contrast computed tomography: initial experiences with a photon counting scanner approved for clinical use. *Diagnostics (Basel)*. 2021;11:2377.
76. Lennartz S, Schoenbeck D, Kröger JR, et al. Photon-counting CT material decomposition: initial experience in assessing adrenal adenoma. *Radiology*. 2023;306:202–204.
77. Niehoff JH, Woeltjen MM, Saeed S, et al. Assessment of hepatic steatosis based on virtual non-contrast computed tomography: initial experiences with a photon counting scanner approved for clinical use. *Eur J Radiol*. 2022;149:110185.
78. Jungblut L, Sartoretti T, Kronenberg D, et al. Performance of virtual non-contrast images generated on clinical photon-counting detector CT for emphysema quantification: proof of concept. *Br J Radiol*. 2022;95:20211367.
79. Emrich T, Aquino G, Schoepf UJ, et al. Coronary computed tomography angiography-based calcium scoring: in vitro and in vivo validation of a novel virtual noniodine reconstruction algorithm on a clinical, first-generation dual-source, photon counting-detector system. *Invest Radiol*. 2022;57:536–543.
80. Allmendinger T, Nowak T, Flohr T, et al. Photon-counting detector CT-based vascular calcium removal algorithm: assessment using a cardiac motion phantom. *Invest Radiol*. 2022;57:399–405.
81. Zsarnóczay E, Varga-Szemes A, Emrich T, et al. Characterizing the heart and the myocardium with photon-counting CT. *Invest Radiol*. 2023. doi:10.1097/RLI.0000000000000956.
82. Wildberger JE, Alkadhi H. New horizons in vascular imaging with photon-counting Detector CT. *Invest Radiol*. 2023. doi:10.1097/RLI.0000000000000957.
83. Symons R, Krauss B, Sahbaee P, et al. Photon-counting CT for simultaneous imaging of multiple contrast agents in the abdomen: an in vivo study. *Med Phys*. 2017;44:5120–5127.
84. Si-Mohamed S, Tatard-Leitman V, Laugerette A, et al. Spectral photon-counting computed tomography (SPCCT): in-vivo single-acquisition, multi-phase liver imaging with a dual contrast agent protocol. *Sci Rep*. 2019;9:8458.
85. Si-Mohamed S, Thivolet A, Bonnot PE, et al. Improved peritoneal cavity and abdominal organ imaging using a biphasic contrast agent protocol and spectral photon counting computed tomography K-edge imaging. *Invest Radiol*. 2018;53:629–639.
86. Jungblut L, Abel F, Nakhostin D, et al. Impact of photon counting detector CT derived virtual monoenergetic images and iodine maps on the diagnosis of pleural empyema. *Diagn Interv Imaging*. 2023;104:84–90.
87. Soschynski M, Hagen F, Baumann S, et al. High temporal resolution dual-source photon-counting, CT for coronary artery disease: initial multicenter clinical experience. *J Clin Med*. 2022;11:6003.
88. Tharmaseelan H, Froelich MF, Nörenberg D, et al. Influence of local aortic calcification on periaortic adipose tissue radiomics texture features—a primary analysis on PCCT. *Int J Cardiovasc Imaging*. 2022;38:2459–2467.
89. Tharmaseelan H, Rotkopf LT, Ayx I, et al. Evaluation of radiomics feature stability in abdominal monoenergetic photon counting CT reconstructions. *Sci Rep*. 2022;12:19594.
90. Ayx I, Tharmaseelan H, Hertel A, et al. Comparison study of myocardial radiomics feature properties on energy-integrating and photon-counting detector CT. *Diagnostics (Basel)*. 2022;12:1294.
91. Ayx I, Tharmaseelan H, Hertel A, et al. Myocardial radiomics texture features associated with increased coronary calcium score-first results of a photon-counting CT. *Diagnostics (Basel)*. 2022;12:1663.